AJR FOCUS ON:

MR Neurography: Past, Present, and Future

Avneesh Chhabra[1]
Gustav Andreisek[2]
Theodoros Soldatos[1]
Kenneth C. Wang[1]
Aaron J. Flammang[1]
Allan J. Belzberg[3]
John A. Carrino[1]

OBJECTIVE. MR neurography (MRN) has increasingly been used in clinical practice for the evaluation of peripheral nerve disease. This article reviews the historic perspective of MRN, the current imaging trends of this modality, and the future directions and applications that have shown potential for improved imaging and diagnostic capabilities.

CONCLUSION. MRN has come a long way in the past 2 decades. Excellent depiction of 3D nerve anatomy and pathology is currently possible. Further technical developments in diffusion-based nerve and muscle imaging, whole-body MRN, and nerve-specific MR contrast agents will likely play a major role in advancing this novel field and understanding peripheral neuromuscular diseases in the years to come.

Clinical evaluation of peripheral neuropathies has traditionally relied on clinical examination and electrodiagnostic testing. MRI of peripheral nerves, also referred to as MR neurography (MRN), is increasingly being used in clinical routine because of advances in MRI hardware and the development of new imaging techniques [1, 2]. MRN nicely depicts peripheral nerve anatomy and pathology [3–7], and studies have shown that MRN findings may substantially influence the management of patients with peripheral neuropathies [8, 9]. Recent technical developments such as diffusion-weighted imaging (DWI) and diffusion-tensor imaging (DTI) are currently being evaluated for imaging of the peripheral nerve system [10, 11]. This article reviews the historic perspective of MRN, the current imaging trends of this technique, and the future directions and applications that have shown potential for improved imaging and diagnostic capabilities.

Role of MR Neurography

MRN provides important information that may assist in the diagnostic and therapeutic workup of peripheral nerve lesions. MRN has been successfully used to confirm clinical suspicion of peripheral neuropathy by directly showing the nerve abnormality or regional muscle denervation changes; to assess the extent of the abnormality in nerve injuries or the disease load in diffuse peripheral nerve lesions, such as hereditary neuropathies and neurofibromatosis; to depict the lesions causing nerve entrapment or impingement; to exclude the diagnosis of neuropathy by showing normal nerves and regional muscles; to detect incidental lesions in the region of interest that mimic neuropathy symptoms; and to provide imaging guidance for perineural medication injections [1–10].

Interpretation of MR Neurography and Classification of Nerve Injury

Axial T1-weighted and fluid-sensitive fat-suppressed T2-weighted images serve as the mainstay in MRN interpretation for prudent assessment of peripheral nerve imaging characteristics, such as signal intensity (SI) evaluation, course, caliber, fascicular pattern, size, and perineural fibrosis or mass lesions [1]. Normal nerves show intermediate SI (similar to muscle) on T1-weighted images and intermediate to minimally increased SI on T2-weighted images, depending on the amount of endoneurial fluid and background fat suppression [12]. In cases of neuropathy, the SI of the nerve increases abnormally, approaching the fluidlike SI of the adjacent vessels, on T2-weighted imaging [13] (Fig. 1). This phenomenon has been explained by various hypothesized mechanisms, such as vascular congestion; blockade of axoplasmic flow, leading to abnormal proximal accumulation of endoneurial fluid; and distal wallerian degeneration changes [6, 14]. Additional MR characteristics

Keywords: MRI, MR neurography, peripheral nerves

DOI:10.2214/AJR.10.6012

Received October 17, 2010; accepted after revision January 18, 2011.

[1]The Russell H. Morgan Department of Radiology and Radiological Science, Johns Hopkins Hospital, 601 N Caroline St, Baltimore, MD 21287. Address correspondence to A. Chhabra (achhabr6@jhmi.edu).

[2]Department of Radiology, University Hospital of Zürich, Zürich, Switzerland.

[3]Department of Neurosurgery, Johns Hopkins Hospital, Baltimore, MD.

AJR 2011; 197:583–591

0361–803X/11/1973–583

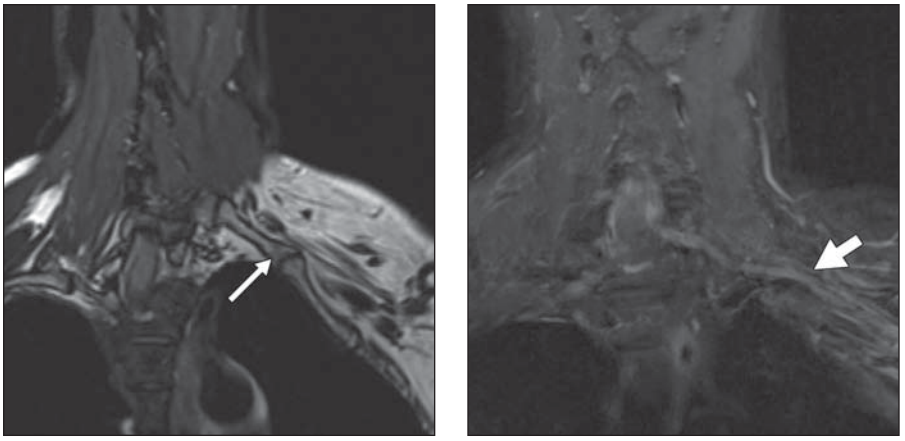

Fig. 1—55-year-old man with left arm and hand pain along lower brachial plexus trunk distribution (suspected thoracic outlet syndrome).
A, Oblique coronal 3D T2 sampling perfection with application optimized contrast (SPACE, Siemens Healthcare) reconstruction image shows anomalous left cervical rib (*arrow*) articulating with first rib.
B, Coronal 3D STIR SPACE reconstruction image shows kinking, displacement, abnormal T2 hyperintensity, and mild enlargement of left C8 nerve root and lower trunk (*arrow*).

of normal and abnormal nerves are outlined in Table 1. Focal alterations in nerve contour, course, and caliber are best depicted on longitudinal images reconstructed along the course of the nerve on dedicated imaging workstations using various techniques, such as multiplanar reconstruction (MPR), curved-planar reconstruction (Fig. 1), and maximum intensity projection [1, 15].

Nerve injuries have been traditionally classified according to Seddon et al. [16] and Sunderland [17] grading systems (Table 2). Seddon et al. divided nerve injuries on the basis of severity into neurapraxia, axonotmesis, and neurotmesis. Pathologic changes in neurapraxia, the mildest type of injury, involve only the myelin sheath around the axon with resultant transient functional loss and are associated with an excellent prognosis. In a neurapraxic injury, MRN shows abnormal T2 hyperintensity and mild enlargement of the peripheral nerve (Fig. 2). In our experience, this milder nerve abnormality can be seen in neurapraxia; mild stretch injury; and other types of mild nerve entrapment, such as tunnel syndromes and compression from space-occupying lesions (Fig. 1).

In axonotmesis, the axon suffers complete rupture resulting in wallerian degeneration of its distal segment; however, the supporting structures, including the perineurium and epineurium, remain intact [4, 6]. The prognosis for recovery remains good, but time is required for axonal regeneration (≈ 1 mm per day) from the point of injury to the target tissue. Based on our experience and surgical correlations, MRN findings include effacement, enlargement, or disruption of individual fascicles in addition to those MRN findings seen in neurapraxia (Fig. 3). Similar MRN changes may be seen with moderate-to-severe nerve entrapment, especially in long-standing cases and repeat tunnel surgeries.

Neurotmesis is the most severe type of injury and refers to complete severance of the nerve. The functional loss is complete, and unless early surgical intervention is performed clinical recovery is not anticipated. In the acute stage of neurotmesis, MRN can directly show the nerve discontinuity and the gap filled with fluid and granulation tissue between the torn nerve endings. Fibrosis at the injury site is typically seen in the subacute and chronic stages as strandy hypointense soft tissue within the nerve gap on T2-weighted imaging.

Sunderland [17] further stratified the classification proposed by Seddon and colleagues [16] into five degrees of nerve injuries on the basis of the severity of the injury. First- and second-degree injuries correspond to neurapraxia and axonotmesis, whereas the third-, fourth-, and fifth-degree injuries involve injury to the endoneurium, perineurium, and epineurium, respectively. In third-degree injuries, the functional recovery depends on the extent of endoneurial damage. The fourth- and fifth-degree nerve injuries require surgery for any possible functional recovery. Based on our ever-increasing experience in an attempt to further define these injuries, MRN typically shows a neuroma in continuity in the fourth-degree cases. Regenerating nerve sprouts, unable to grow down the disrupted fascicles, tangle in conjunction with perifascicular and intrafascicular fibrosis to form this neuroma, which is seen in continuity with the proximal and distal uninvolved nerve segments [1] (Fig. 4). Complete nerve discontinuity in fifth-degree injury is also well depicted on MRN (Fig. 5). On MRN, neuroma is seen as focal nerve enlargement with a partially or completely effaced fasicular pattern.

In addition to the direct nerve-related MRN signs, muscle SI changes on MR images can indicate or can further confirm the presence of neuropathy. These denervation-related MR signal abnormalities have been shown to be a relative shift between intra- and extracompartmental fluid components and do not reflect real edema. Muscles may show acute denervation changes (edemalike SI) as early as 24 hours from the onset of neuropathy;

TABLE 1: MR Neurography Interpretation of Peripheral Nerve Injuries

Feature	Normal Nerve	Abnormal Nerve
Size	Similar to adjacent arteries, gradually decreases distally	Focal or diffuse enlargement, larger than adjacent arteries
Signal intensity	Isointense to skeletal muscle on T1- and T2-weighted imaging; isointense to minimally hyperintense on STIR and fat-suppressed T2-weighted imaging	Hyperintense on T2-weighted imaging similar to adjacent veins
Fascicular pattern	Present on T1- and T2-weighted imaging	Enlargement or disruption of single or multiple fascicles
Course	Smooth without focal deviations, outlined by perineural fat	Focal or diffuse deviations, discontinuity
Enhancement	Absent except in areas of deficient blood-nerve barrier, such as dorsal nerve root ganglion	Present in tumors and infections because of disruption of blood-nerve barrier
Perineural fat planes	Preserved and clean	Effaced

TABLE 2: Classifications of Nerve Injuries

Classification System [Reference No.]		Neural Structures Affected by Injury				
Seddon et al. [16]	Sunderland [17]	Myelin	Axon	Endoneurium	Perineurium	Epineurium
I	Neurapraxia	—				
II	Axonotmesis	Yes/no	Yes	No	No	No
III	NA	Yes	Yes	Yes	No	No
IV	NA	Yes	Yes	Yes	Yes	No
V	Neurotmesis	Yes	Yes	Yes	Yes	Yes

Note—Dash (—) indicates that only myelin sheath around the axon is involved. NA = not applicable.

subacute changes (edemalike SI and minimal fatty replacement), weeks to months after injury; or chronic changes (fatty replacement and atrophy), months to years after nerve injury [5] (Fig. 6B). If the muscles show severe fatty replacement, it is unlikely that primary nerve repair will yield satisfactory results. In those cases, free muscle or tendon transfers may be attempted for better recovery. In some cases, denervation changes may be difficult to differentiate from systemic or metabolic myopathy or exercise-induced changes. However, the presence of muscle changes in a regional nerve distribution, diffuse rather than focal muscle involvement, and lack of fascial and subcutaneous edema help in the differentiation of denervation from other causes, such as infectious or traumatic myopathy.

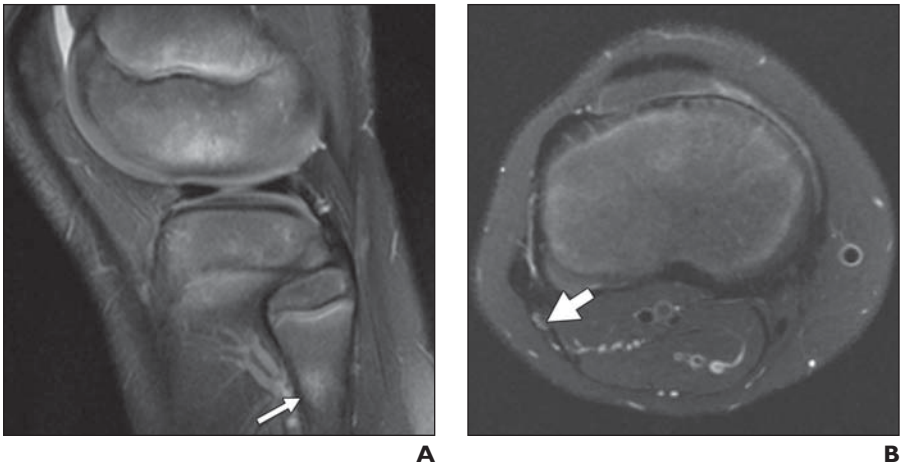

Fig. 2—8-year-old girl with persistent left leg pain after buckle fracture of proximal fibula.
A, Sagittal fat-suppressed T2-weighted image shows bone marrow edema (*arrow*) and cortical buckling at fracture site.
B, Coronal fat-suppressed T2-weighted image shows mild abnormal T2 hyperintensity of common peroneal nerve (*arrow*) without fascicular enlargement in case of neurapraxia (mild nerve injury).

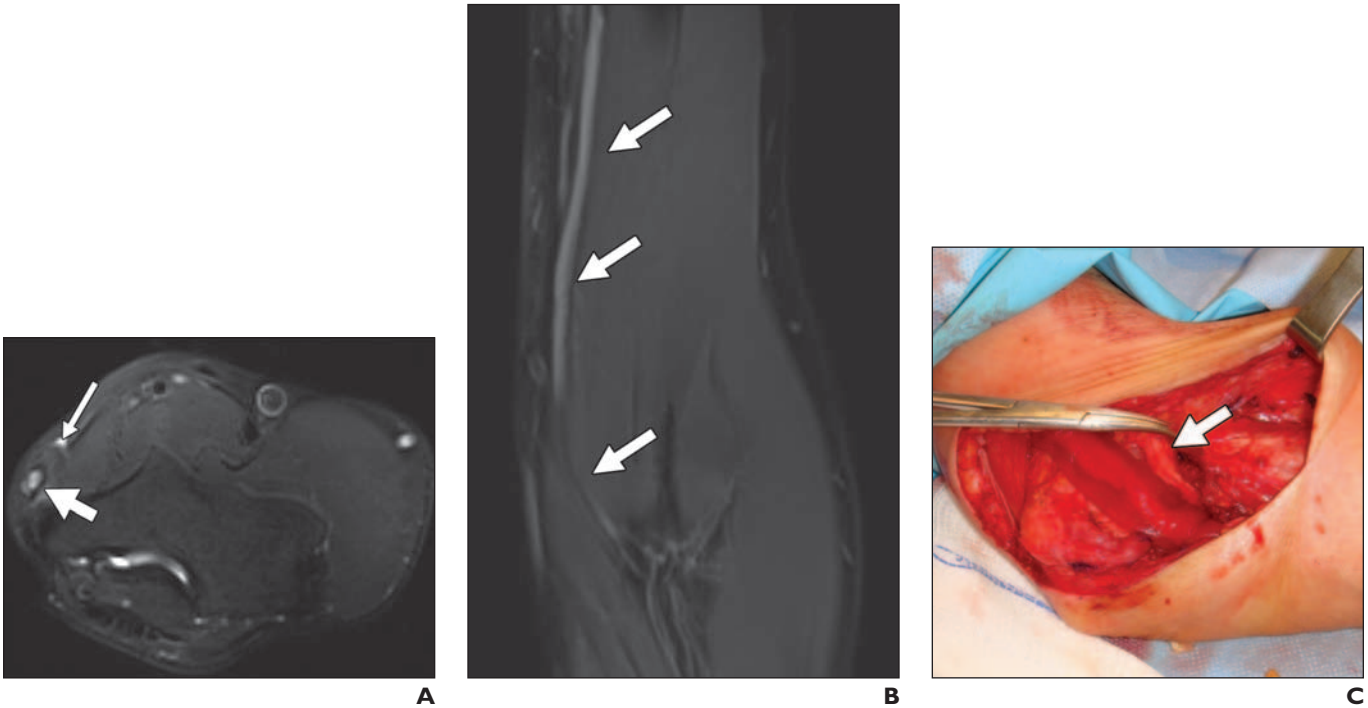

Fig. 3—52-year-old woman with previous anterior submuscular transposition of ulnar nerve.
A, Axial T2 spectrally adiabatic inversion recovery (SPAIR, Siemens Healthcare) image obtained just distal to medial epicondyle shows two enlarged fascicles within mildly enlarged ulnar nerve (*thick arrow*), which is located in subfascial position. Notice that fascicular T2 hyperintensity is similar to adjacent vessel (*thin arrow*).
B, Coronal STIR image shows abnormally enlarged and T2 hyperintense ulnar nerve (*arrows*). Because of persistent symptoms, patients underwent neurolysis.
C, Intraoperative photograph confirms enlargement of individual fascicles (*arrow*) just distal to medial epicondyle in this case of axonotmesis.

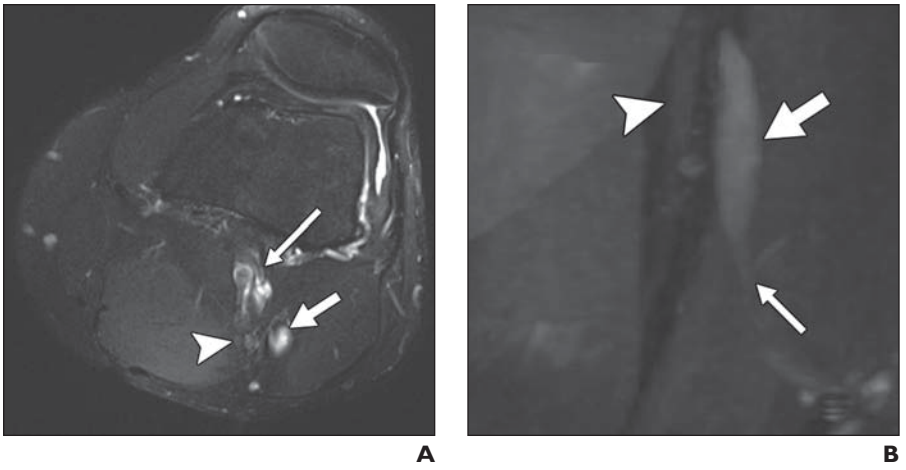

Fig. 4—23-year-old man who presented with worsening foot drop and posterior calf pain a few months after posterolateral corner injury of knee.
A, Axial T2 spectrally adiabatic inversion recovery (SPAIR, Siemens Healthcare) image obtained at level of popliteal fossa shows mildly T2 hyperintense tibial nerve (*arrowhead*, mild stretch injury proven on electromyography) and markedly abnormal, enlarged common peroneal nerve (*thick arrow*) with disrupted fascicles and T2 hyperintensity similar to anteriorly located vessels (*thin arrow*).
B, Coronal reconstructed maximum-intensity-projection image from fat-suppressed 3D diffusion-weighted PSIF (reversed FISP [fast imaging with steady-state free precession]) sequence depicts large neuroma in continuity (*thick arrow*) involving common peroneal nerve (*thin arrow*). Tibial nerve is identified by *arrowhead*.

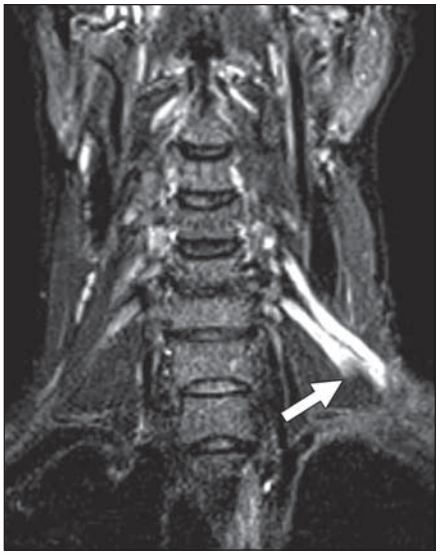

Fig. 5—43-year-old woman who presented with dense neurologic deficit after left neck dissection. Coronal reconstruction from 3D STIR sampling perfection with application optimized contrast (SPACE, Siemens Healthcare) image of brachial plexus confirms left upper trunk transection (*arrow*), which is considered Sunderland fifth-degree injury. Notice enlarged and T2 hyperintense C5 and C6 nerve roots. Patient subsequently underwent nerve grafting.

The Past: Historic Perspective and Applications of MR Neurography

An electrodiagnostic study, which includes electromyography and nerve conduction examinations, has been widely considered the reference method for the diagnosis of peripheral neuropathy. However, an electrodiagnostic study is time-consuming to perform; may provide indeterminate results, especially in postoperative cases because of the long delay of electrical signals to return; may be uncomfortable for patients; or may even be unfeasible in subjects with dermatologic diseases and in cases of inaccessible deeply situated nerves [18, 19]. In addition, an electrodiagnostic study may not reveal the exact site of nerve injury and is unable to detect neuromas or distinguish between adhesive (perineural fibrosis) and compressive mass lesions.

MRN and ultrasound were introduced in the 1980s as noninvasive techniques that could address some of the aforementioned issues [20–22]. Ultrasound is useful for the assessment of superficial peripheral nerves, is inexpensive, and enables dynamic imaging and easy differentiation of nerves from vessels using Doppler imaging. On the other hand, ultrasound remains operator-dependent and nerve imaging may be degraded by dense scarring and shadowing from surrounding calcifications. The latter issue becomes prominent in cases of deeply situated nerves, especially of the pelvis and lumbosacral plexus [23]. Compared with ultrasound, MRN is not operator-dependent, provides higher soft-tissue contrast with depiction of subtle T2 signal abnormalities, and offers more objective visualization of a nerve abnormality and of abnormalities in surrounding tissues. Additionally, secondary muscle denervation changes are better depicted on MRN examinations.

In the past 2 decades, several review articles and a limited number of original scientific studies have described the application of MRN on 1.5-T and lower-field-strength scanners. Historically, compared with an electrodiagnostic study, MRN exhibited good diagnostic accuracy for nerve sheath tumors and only moderate diagnostic accuracy in the evaluation of compressive neuropathies, such as carpal and cubital tunnel syndromes [24, 25]. This limitation was related to the low available imaging resolution and contrast provided by the equipment of that time [26].

From a review of the radiology literature, it may be inferred that fat suppression was inconsistently used because of the long imaging times demanded by low-field-strength magnets [3, 4, 6]. Because suboptimal or no fat saturation was applied for T2-weighted imaging, the abnormal signal within the nerve could have been easily obscured by the hyperintense T2 signal of the adjacent fat. In some of these studies, a STIR sequence was frequently used to obtain fluid-sensitive images with uniform fat suppression [24, 27]. However, STIR images require long acquisition times, have poor spatial resolution, and may be degraded by pulsation artifacts (Fig. 7A). Additionally, peripheral nerves and vessels display similar MR signal characteristics on STIR images and their differentiation within the neurovascular bundle may be difficult (Fig. 7B). The latter limitation is often prominent on MRN studies of the extremities—where small peripheral nerves may not be differentiated from adjacent veins. Furthermore, an attempt to suppress vascular signal with saturation bands often fails in distal locations of the body because the neurovascular bundles frequently course through various obliquities [27, 28]. Additionally, large-FOV imaging of structures, such as the brachial plexus and sciatic nerves, is limited on low-field scanners because of nonuniform fat suppression. Three-dimensional imaging is also markedly degraded on low-field scanners because only gradient-echo 3D sequences were feasible on the equipment of that era to avoid a time penalty. These sequences were also characterized by suboptimal signal-to-noise ratio, lower contrast-to-noise ratio, increased sensitivity to susceptibility artifacts, and nonisotropic multiplanar reformats.

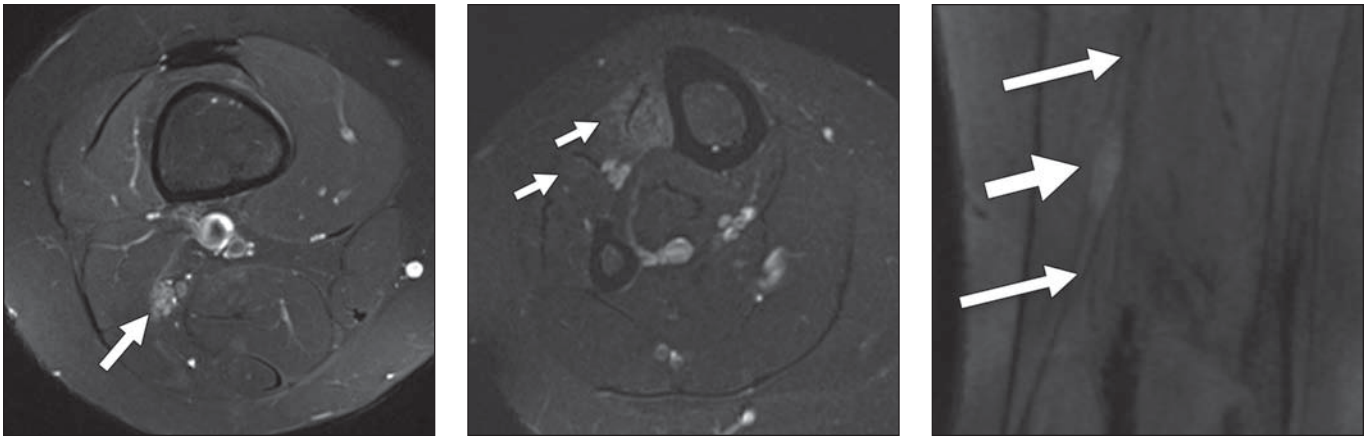

Fig. 6—13-year-old boy who presented with foot drop of many months' duration.
A and **B,** Sequential axial T2 spectrally adiabatic inversion recovery (SPAIR, Siemens Healthcare) images show abnormally enlarged common peroneal component of sciatic nerve with enlarged fascicles (*arrow*, **A**) in biopsy-proven perineuroma. Anterior compartment denervation changes (*arrows*, **B**) are shown in distal image.
C, Coronal reconstruction from fat-suppressed diffusion-weighted PSIF (reversed FISP [fast imaging with steady-state free precession]) image nicely depicts perineuroma (*thick arrow*) arising out of common peroneal nerve (*thin arrows*) with selective vascular suppression of vessels and fat.

The Present: Current Concepts and Applications of MR Neurography

The recent advances and enhancements of MRN techniques have surpassed several diagnostic challenges of the past. The increasing use of 3-T MR scanners, new phased-array surface coils, and parallel imaging aids in the acquisition of high-resolution and high-contrast images in short imaging times. Current state-of-the-art MRI provides detailed anatomic depiction of peripheral nerves and improved characterization of pathologic states [29–31]. It is now possible, for example, to discriminate which particular small elements of the brachial plexus are involved in tumors or neuropathies (Fig. 8). Larger regions of the body can be imaged using large FOVs with uniform magnet homogeneity, even in off-center areas. In addition, frequent use of water-selective fat-saturation (Dixon) techniques provides more robust fat suppression (Fig. 6C).

On the basis of clinical and electrodiagnostic study findings, referring physicians are usually able to determine the anatomic area to be imaged. In certain cases, however, this preselection of FOV is not possible. In those cases, multiple areas of the body can be quickly screened using T1-weighted and STIR images at a lower spatial resolution. However, the prospectively determined target areas should always be evaluated using high-resolution MRN sequences.

Multidisciplinary conferences with participation of referring physicians, neurologists, radiologists, and MR technologists are routinely conducted at our institute. These conferences are particularly useful for discussing imaging, clinical, and electrodiagnostic study findings in patients who have recently undergone MRN examination and for tailoring the MRN imaging protocol (e.g., anatomic area, imaging planes) in a future patient.

The high-resolution MRN protocol should encompass 2D and 3D techniques. Axial 2D T1-weighted spin-echo and T2-weighted spectrally adiabatic inversion recovery (SPAIR, Siemens Healthcare) turbo spin-echo images provide excellent depiction of a nerve with intermediate SI. Compared with STIR, T2-weighted SPAIR imaging not only is more favorable with regard to the specific absorption rate, but also yields a higher signal-to-noise ratio on 3-T MRI. In addition, T2-weighted SPAIR images provide more homogeneous fat suppression than frequency-selective T2 fat-suppressed images in off-center areas [1]. Individual fascicular enlargement, abnormal T2 hyperintensity, and disruption or effacement of the fascicular appearance are easily depicted on these images (Figs. 3A and 4A).

Misinterpretations related to magic angle effect artifacts causing T2 hyperintensity can be avoided by reviewing images obtained with increased TE values (> 60 ms). A variety of 3D sequences with predominant spin-echo–type contrast are available in the current 3-T MRN

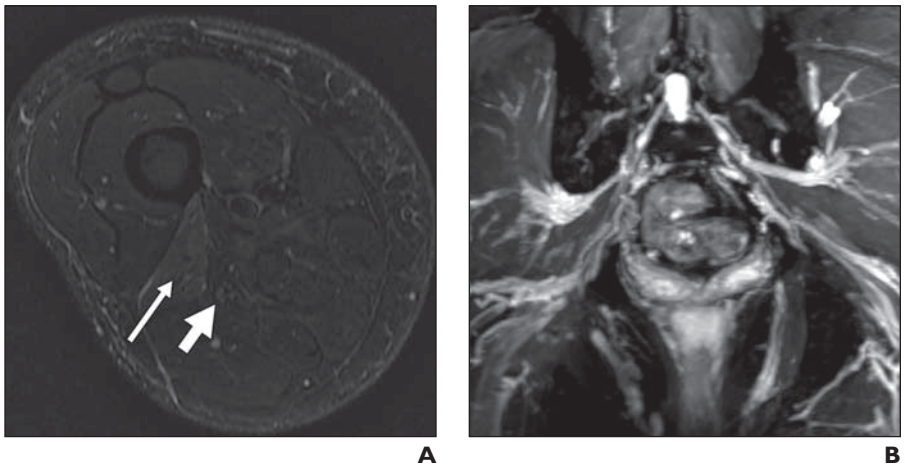

Fig. 7—MR neurography images acquired on 1.5-T scanners.
A, Axial STIR image through distal thigh of 63-year-old man with foot drop after having undergone right hip replacement shows denervation changes involving biceps femoris muscle (*thin arrow*). Notice poor depiction of peroneal nerve abnormality (*thick arrow*) related to suboptimal signal-to-noise ratio.
B, Coronal STIR image of 43-year-old woman with sciatic neuropathy shows poor differentiation of sciatic nerve from adjacent gluteal neurovascular bundles.

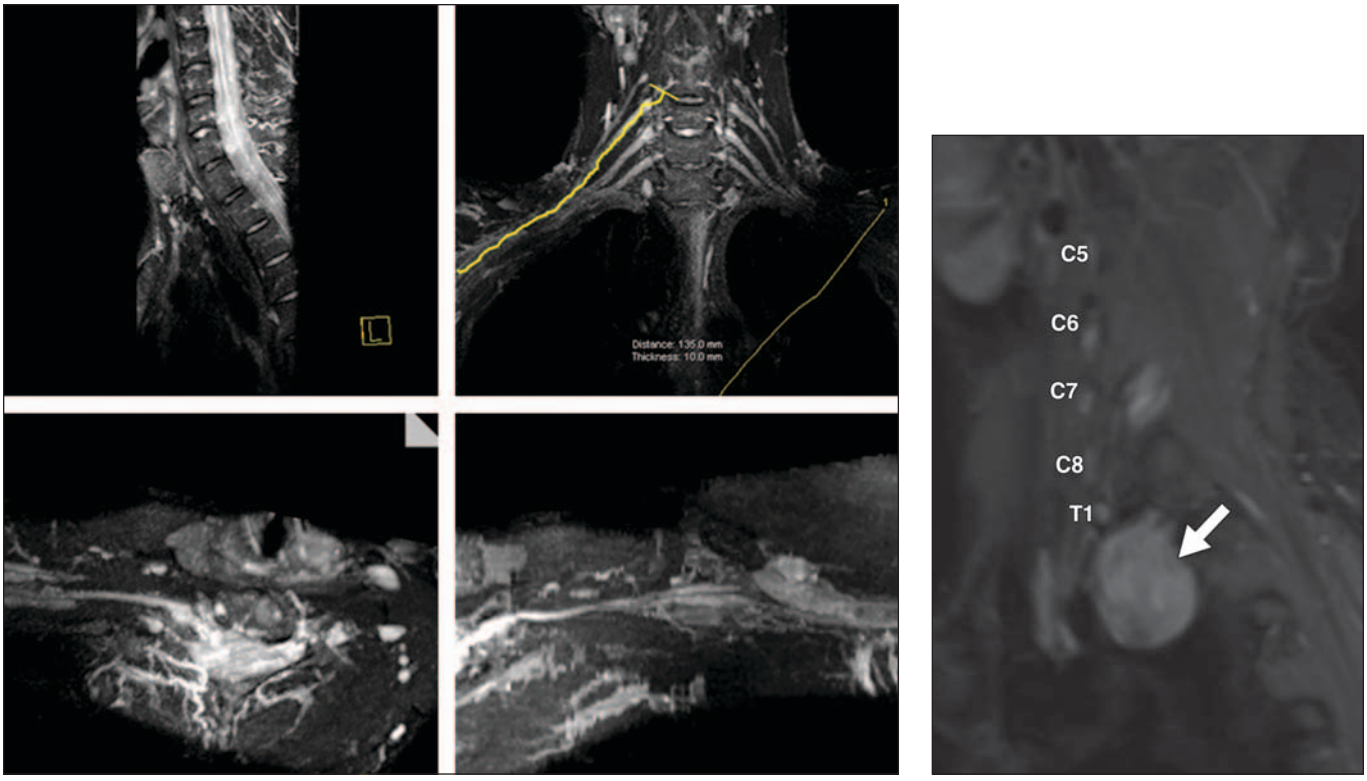

Fig. 8—Reconstruction images obtained from 3D MR neurography sequences.
A, Multiplanar isotropic reformation images from 3D STIR sampling perfection with application optimized contrast (SPACE, Siemens Healthcare) sequence depict various individual segments of brachial plexus in healthy 38-year-old male volunteer.
B, 40-year-old woman with known schwannoma diagnosed on MRI at another institution. Sagittal reconstruction image from 3D STIR SPACE sequence obtained as part of preoperative planning shows lesion (*arrow*) arising from T2 nerve root sheath in lower aspect of scalene triangle and displacing left T1 nerve root anterosuperiorly.

armamentarium. These sequences provide isotropic spatial resolution of 0.4–0.8 mm. In our institute, high-resolution and high-contrast isotropic 3D images (e.g., T2 SPACE [sampling perfection with application optimized contrast, Siemens Healthcare] and STIR SPACE) are routinely obtained, allowing MPRs and curved-planar reconstructions along the long axis of the peripheral nerves, which course through a variety of obliquities (Figs. 1, 5, 8, and 9). High-resolution and high-contrast isotropic 3D images can display even subtle alterations in nerve contour, caliber, and SI.

Images reformatted in longitudinal planes have proven valuable in surgical planning and can provide intraoperative references on or adjacent to the nerves and the plexuses [1, 31]. In addition, we frequently use fat-suppressed 3D DW PSIF (reversed FISP [fast imaging with steady-state free precession]) imaging sequences for peripheral nerve imaging in the extremities (Figs. 4B and 6C). Besides retaining all the advantages of a 3D sequence, 3D DW PSIF provides selective suppression of all moving structures, including vascular flow, thereby enabling selective visualization of the nerves [32].

The current imaging protocol encompassing axial 2D T1-weighted (3-mm isotropic reconstructions), axial T2 SPAIR (3 mm), coronal 3D STIR SPACE and T2 SPACE (1 mm), and 3D DW PSIF imaging (1 mm) can be accomplished within 45 minutes of imaging time. The use of IV contrast material (i.e., gadolinium) for extremity and plexus neurographies in our practice is generally restricted to cases of suspected infections, inflammations, diffuse peripheral nerve lesions, and tumors [33]. Injured and entrapped nerves and posttraumatic neuromas generally show abnormal T2 hyperintensity on unenhanced images, whereas contrast-enhanced images do not add much value except in showing enhancement in the denervated muscles [1].

Using this high-resolution MRN protocol, neuromas in continuity and nerve discontinuities are easily depicted, thereby helping referring physicians make a diagnosis of Sunderland fourth- and fifth-degree nerve injuries, respectively (Figs. 4, 5, and 9). Isolated deep bundle neuritis in cases of ulnar neuropathy and relative involvement of various bundles of the median nerve or components of the sciatic nerve are adequately depicted (Figs. 4 and 6). The reconstructed true axial images provide improved visualization of the internal architecture at any point along the course of the nerves. Three-dimensional imaging is also a prudent way to look at nerve distortions related to disk herniations and in kyphoscoliotic curvatures of the spine [15]. Muscle variations and volumes are also better assessed on 3D imaging, especially in cases of piriformis or thoracic outlet syndrome, because arbitrary MPR at a postprocessing workstation allows the precise plane adjustment required for accurate side-by-side comparisons.

Because of the increasing number of peripheral nerve microsurgeries for nerve injuries and the advanced current imaging capabilities of MRN, there has been a growing demand for postoperative imaging to evaluate the regeneration of small peripheral nerves through nerve tubes and assess persistent nerve discontinui-

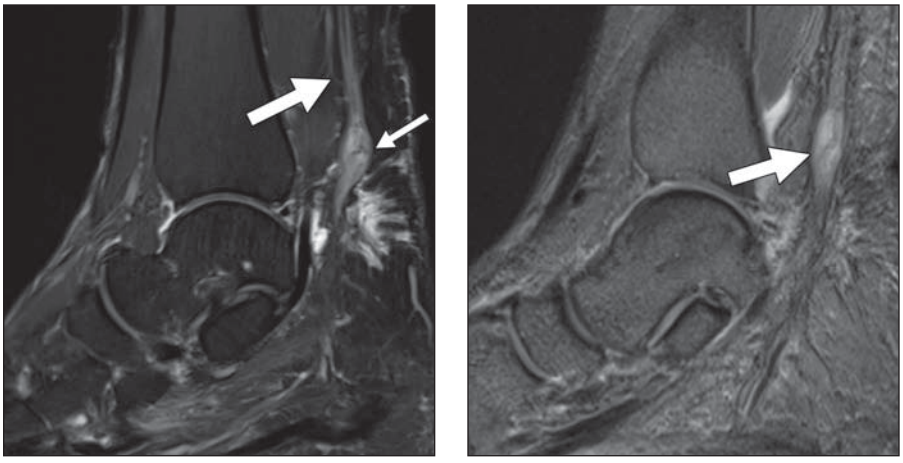

Fig. 9—46-year-old woman with neuroma in continuity after prior tibial nerve injury.
A, Sagittal STIR image shows neuroma in continuity (*thick arrow*) arising from tibial nerve (*thin arrow*).
B, After neurolysis, collagen-based wrap was placed around nerve, seen as T2 hypointensity on sagittal reconstruction image from 3D T2 sampling perfection with application optimized contrast (SPACE, Siemens Healthcare) sequence. Despite reduction of neuroma size and clinical improvement, there is persistent abnormal T2 hyperintensity of lesion (*arrow*).

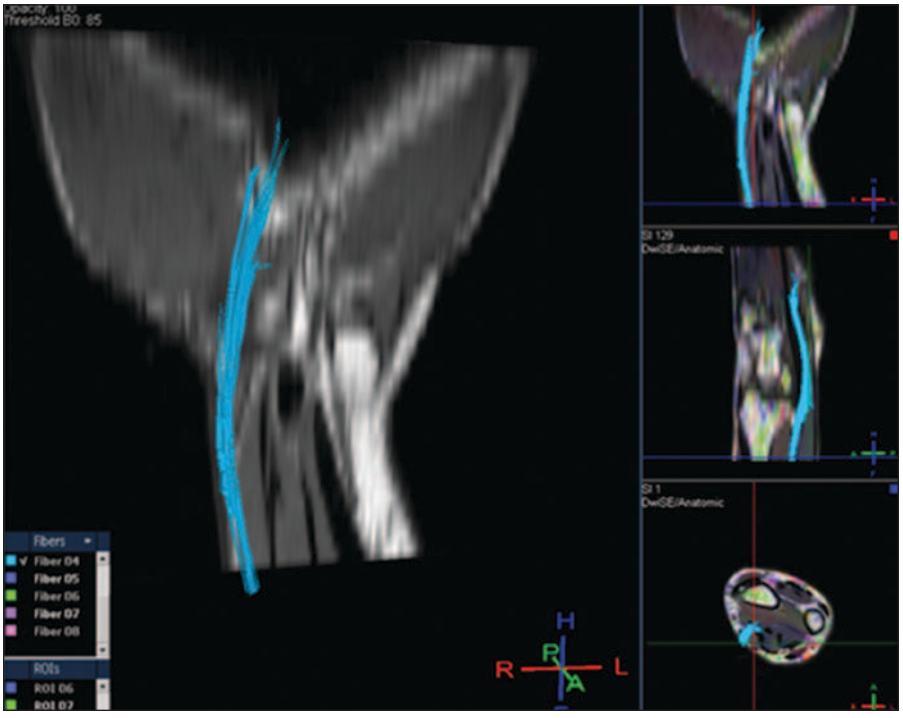

Fig. 10—Future directions in MR neurography.
A, Three-dimensional median nerve tractography of healthy 35-year-old male volunteer using b value of 1000 s/mm^2 and 25 directions of interrogation. Notice multiplanar isotropic visualization of median nerve tracts (*blue*). A = anterior, P = posterior, H = head.
B, MR-guided intervention in 45-year-old woman with left-sided pudendal neuralgia. Axial T2 fat-suppressed image shows MR-compatible needle with surrounding T2 hyperintense medication (*arrow*) filling Alcock canal. Nerve is not separately visualized.
C, Axial diffusion image of 34-year-old man obtained from diffusion-tensor imaging sequence shows surgically confirmed entrapped radial nerve (*arrow*) at spiral groove. Parametric analysis shows abnormally low fractional anisotropy and high apparent diffusion coefficient values along course of nerve.
D, Axial fat-suppressed T2 MR image obtained on 7-T scanner of median nerve from cadaver specimen. There is clear delineation of individual fascicles (*arrow*) of median nerve.

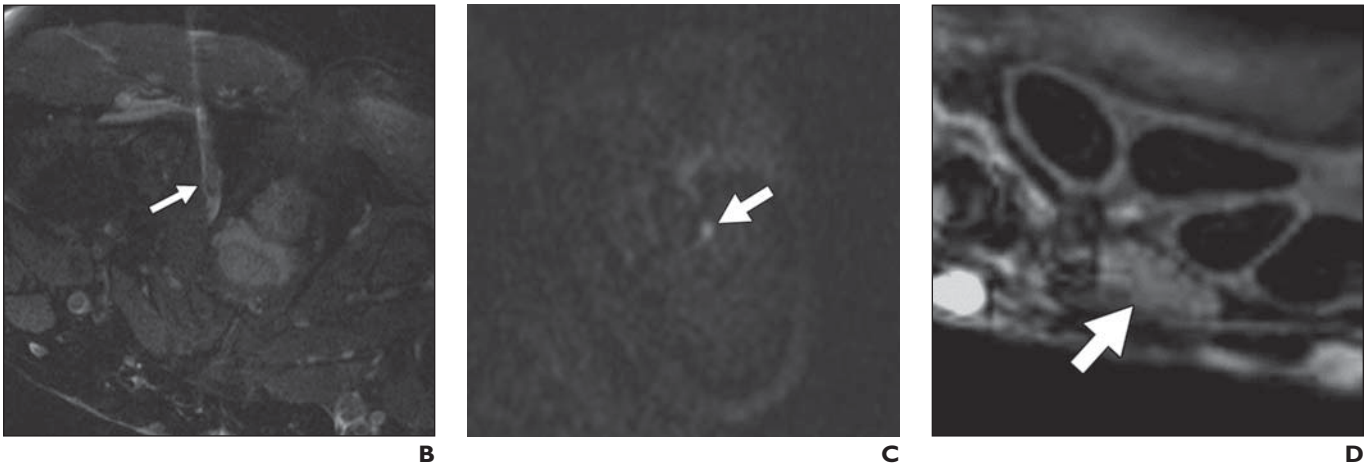

ty or neuroma formation at repair sites [1, 27]. After nerve entrapment surgery, T2 hyperintensity usually normalizes within 8 weeks after neurolysis [27, 34, 35]. The presence of one or more imaging findings—such as persistent nerve enlargement, abnormal T2 hyperintensity approaching the SI of adjacent vessels, encasing perineural fibrosis, and fascicular abnormality—suggests reentrapment [36] (Fig. 3). In some cases, however, a T2 signal abnormality may persist for prolonged time periods despite clinical improvement; therefore, other morphologic signs of nerve abnormality should be evaluated before making the diagnosis of persistent neuropathy (Fig. 9). In addition, current T2-based MRI still provides limited evaluation of nerve regeneration, and more physiologic (functional) assessment is warranted in the future for the confident diagnosis of reinnervation.

Recently, there has been considerable research using diffusion-based imaging for nerve identification in human studies. Encouraging results have been seen with the application of DTI in animal models for the assessment of nerve regeneration and with the application of tractography in healthy human volunteers [11, 37–39] (Fig. 10A).

MR-guided nerve intervention has also been increasingly used in clinical practice. MRN affords reliable localization of the abnormality before a targeted fascicular biopsy is performed. Radiologists should ensure accurate description of the lesion and of its relationship to the surrounding structures so that the physician may confidently plan the biopsy approach. In some practices, MR-guided perineural injections are routinely and successfully performed with satisfactory results [9, 40] (Fig. 10B).

Future Directions and Applications of MR Neurography

Although MRN has evolved into a highly sensitive technique, its specificity for neuropathies has been questioned [12, 24]. Various diagnostic challenges remain, such as the interpretation of mild T2 hyperintensity of the peripheral nerves as an isolated sign of neuropathy. Mild T2 hyperintensity within the nerve can often be observed in asymptomatic subjects, probably related to magic angle effect, or may represent subclinical neuropathy [12, 41]. Additionally, it is often not possible to distinguish between regenerating and chronically degenerating nerves [42]. Nerves can regrow at a rate of about 1 mm per day, so clinical recovery may require several months. Postoperatively, the electrical activity from reinnervation is also usually delayed, which may complicate the interpretations of electrodiagnostic studies.

We hope that future research using DWI and especially DTI will provide more physiologic information and increase the specificity of MRN in detecting nerve regeneration. DTI allows interrogation of the nerve microstructure and function in addition to providing information on fibers trajectory. Normally, the diffusion of protons along the nerve is three times higher than across the nerve because of restrictions posed by the myelin sheath, a phenomenon also referred to as anisotropy. Thereby, DTI allows nerve tractography and the calculation of quantitative parameters such as the apparent diffusion coefficient (ADC), which describes the mean diffusivity, and fractional anisotropy.

Blockade of the axoplasmic flow or venous congestion and distal wallerian degeneration lead to widening of the potential space between axons and the surrounding covering, resulting in increased proton diffusion and consequently increased ADC and decreased fractional anisotropy values [10] (Fig. 10C). Various nerve abnormalities and injuries, such as trauma, entrapment, tumor, and inflammation, may lead to decreased fractional anisotropy and increased ADC values; therefore, these findings should be taken in the context of morphologic nerve findings on MRN studies along with the available clinical information. Increasing fractional anisotropy values within the peripheral nerves has also been shown in animal models to correlate with motor and sensory functional recovery and may depict nerve regeneration after successful release of the entrapment [10, 40].

The application of higher b values of approximately 1000–1200 s/mm^2 is essential for optimal DTI of the peripheral nerves [43] (Fig. 10A). This novel imaging technique has the potential to depict early signs of nerve regeneration in the proximal aspects of the nerves—well before the first regenerative motor units reach the regional muscles. Additionally, muscle DTI and elastography have shown potential for the noninvasive assessment of the morphologic and elastic properties of skeletal muscle [44, 45]. With future research, these techniques will likely play an important role in the evaluation and further understanding of neuromuscular diseases. Whole-body MRN is technically challenging to perform [46]. However, it may have significant potential in assessing disease load and treatment response in cases of diffuse peripheral nerve lesions and neurofibromatosis.

New MR contrast agents, such as gadoflouride M, have shown potential to assess demyelination and remyelination in peripheral nerves, as shown in an animal model [47]. Gadoflouride M selectively accumulates in nerve fibers undergoing wallerian degeneration and disappears with remyelination. Finally, 7- and 9-T MRN with higher gradient amplitudes and slew rates will be available in the future with a potential for further improvement in soft-tissue contrast, signal, and spatial resolution (Fig. 10D).

In conclusion, MRN has come a long way in the past 2 decades. Excellent depiction of 3D nerve anatomy and pathology is currently possible. Further technical developments in diffusion-based nerve and muscle imaging, whole-body MRN, and nerve-specific MR contrast agents will likely play a major role in advancing this novel field and understanding peripheral neuromuscular disease in years to come.

References

1. Chhabra A, Williams EH, Wang KC, Dellon AL, Carrino JA. MR neurography of neuromas related to nerve injury and entrapment with surgical correlation. *AJNR* 2010; 31:1363–1368
2. Andreisek G, Crook DW, Burg D, Marincek B, Weishaupt D. Peripheral neuropathies of the median, radial and ulnar nerves: MR imaging features. *RadioGraphics* 2006; 26:1267–1287
3. Howe FA, Filler AG, Bell BA, Griffiths JR. Magnetic resonance neurography. *Magn Reson Med* 1992; 28:328–338
4. Filler AG, Howe FA, Hayes CE, et al. Magnetic resonance neurography. *Lancet* 1993; 341:659–661
5. Bendszus M, Koltzenburg M, Wessig C, Solymosi L. Sequential MR imaging of denervated muscle: experimental study. *AJNR* 2002; 23:1427–1431
6. Filler AG, Kliot M, Howe FA, et al. Application of magnetic resonance neurography in the evaluation of patients with peripheral nerve pathology. *J Neurosurg* 1996; 85:299–309
7. Bendszus M, Wessig C, Reiners K, Bartsch AJ, Solymosi L, Koltzenberg M. MR imaging in the differential diagnosis of neurogenic foot drop. *AJNR* 2003; 24:1283–1289
8. Andreisek G, Burg D, Studer A, Weishaupt D. Upper extremity peripheral neuropathies: role and impact of MR imaging on patient management. *Eur Radiol* 2008; 18:1953–1961
9. Filler AG, Haynes J, Jordan SE, et al. Sciatica of nondisc origin and piriformis syndrome: diagnosis by magnetic resonance neurography and interventional magnetic resonance imaging with outcome study of resulting treatment. *J Neurosurg Spine*

2005; 2:99–115
10. Takagi T, Nakamura M, Yamada M, et al. Visualization of peripheral nerve degeneration and regeneration: monitoring with diffusion tensor tractography. *Neuroimage* 2009; 44:884–892
11. Iba K, Wada T, Tamakawa M, Aoki M, Yamashita T. Diffusion-weighted magnetic resonance imaging of the ulnar nerve in cubital tunnel syndrome. *Hand Surg* 2010; 15:11–15
12. Husarik DB, Saupe N, Pfirrmann CW, Jost B, Hodler J, Zanetti M. Elbow nerves: MR findings in 60 asymptomatic subjects—normal anatomy, variants, and pitfalls. *Radiology* 2009; 252:148–156
13. Petchprapa CN, Rosenberg ZS, Sconfienza LM, Cavalcanti CF, Vieira RL, Zember JS. MR imaging of entrapment neuropathies of the lower extremity. Part 1. The pelvis and hip. *RadioGraphics* 2010; 30:983–1000
14. Peled S, Cory DG, Raymond SA, Kirschner DA, Jolesz FA. Water diffusion, T(2), and compartmentation in frog sciatic nerve. *Magn Reson Med* 1999; 42:911–918
15. Zhang Z, Song L, Meng Q, et al. Morphological analysis in patients with sciatica: a magnetic resonance imaging study using three-dimensional high-resolution diffusion-weighted magnetic resonance neurography techniques. *Spine (Phila Pa 1976)* 2009; 34:E245–E250
16. Seddon HJ, Medawar PB, Smith H. Rate of regeneration of peripheral nerves in man. *J Physiol* 1943; 102:191–215
17. Sunderland S. A classification of peripheral nerve injuries producing loss of function. *Brain* 1951; 74:491–516
18. Jablecki CK, Andary MT, So YT, Wilkins DE, Williams FH. Literature review of the usefulness of nerve conduction studies and electromyography for the evaluation of patients with carpal tunnel syndrome: AAEM Quality Assurance Committee. *Muscle Nerve* 1993; 16:1392–1414
19. Dellon AL. Management of peripheral nerve problems in the upper and lower extremity using quantitative sensory testing. *Hand Clin* 1999; 15: 697–715
20. Middleton WD, Kneeland JB, Kellman GM, et al. MR imaging of the carpal tunnel: normal anatomy and preliminary findings in the carpal tunnel syndrome. *AJR* 1987; 148:307–316
21. Weiss KL, Beltran J, Shamam OM, Stilla RF, Levey M. High-field MR surface-coil imaging of the hand and wrist. Part I. Normal anatomy. *Radiology* 1986; 160:143–146
22. Martinoli C, Bianchi S, Gandolfo N, Valle M, Simonetti S, Derchi LE. US of nerve entrapments in osteofibrous tunnels of the upper and lower limbs. *RadioGraphics* 2000; 20(spec no):S199–S213; discussion, S213–S217
23. Gruber H, Peer S, Kovacs P, Marth R, Bodner G. The ultrasonographic appearance of the femoral nerve and cases of iatrogenic impairment. *J Ultrasound Med* 2003; 22:163–172
24. Jarvik JG, Yuen E, Haynor DR, et al. MR nerve imaging in a prospective cohort of patients with suspected carpal tunnel syndrome. *Neurology* 2002; 58:1597–1602
25. Britz GW, Haynor DR, Kuntz C, et al. Ulnar nerve entrapment at the elbow: correlation of magnetic resonance imaging, clinical, electrodiagnostic, and intraoperative findings. *Neurosurgery* 1996; 38:458–465; discussion, 465
26. Zhang H, Xiao B, Zou T. Clinical application of magnetic resonance neurography in peripheral nerve disorders. *Neurosci Bull* 2006; 22:361–367
27. Filler AG, Maravilla KR, Tsuruda JS. MR neurography and muscle MR imaging for image diagnosis of disorders affecting the peripheral nerves and musculature. *Neurol Clin* 2004; 22:643–682
28. Kuntz C 4th, Blake L, Britz G, et al. Magnetic resonance neurography of peripheral nerve lesions in the lower extremity. *Neurosurgery* 1996; 39:750–756; discussion, 756–757
29. Freund W, Brinkmann A, Wagner F, et al. MR neurography with multiplanar reconstruction of 3D MRI datasets: an anatomical study and clinical applications. *Neuroradiology* 2007; 49:335–341
30. Viallon M, Vargas MI, Jlassi H, Lövblad KO, Delavelle J. High-resolution and functional magnetic resonance imaging of the brachial plexus using an isotropic 3D T2 STIR (short term inversion recovery) SPACE sequence and diffusion tensor imaging. *Eur Radiol* 2008; 18:1018–1023
31. Vargas MI, Viallon M, Nguyen D, Beaulieu JY, Delavelle J, Becker M. New approaches in imaging of the brachial plexus. *Eur J Radiol* 2010; 74:403–410
32. Zhang Z, Meng Q, Chen Y, et al. 3-T imaging of the cranial nerves using three-dimensional reversed FISP with diffusion-weighted MR sequence. *J Magn Reson* Imaging 2008; 27:454–458
33. Thawait SK, Chaudhry V, Thawait GK, et al. High-resolution MR neurography of diffuse peripheral nerve lesions. *AJNR* 2010 Nov 24 [Epub ahead of print]
34. Dailey AT, Tsuruda JS, Filler AG, Maravilla KR, Goodkin R, Kliot M. Magnetic resonance neurography of peripheral nerve degeneration and regeneration. *Lancet* 1997; 350:1221–1222
35. Cudlip SA, Howe FA, Griffiths JR, Bell BA. Magnetic resonance neurography of peripheral nerve following experimental crush injury, and correlation with functional deficit. *J Neurosurg* 2002; 96:755–759
36. Chhabra A, Subhawong TK, Williams EH, et al. High-resolution MR neurography: evaluation before repeat tarsal tunnel surgery. *AJR* 2011; 197:175–183
37. Takahara T, Hendrikse J, Yamashita T, et al. Diffusion-weighted MR neurography of the brachial plexus: feasibility study. *Radiology* 2008; 249: 653–660
38. Jambawalikar S, Baum J, Button T, Li H, Geronimo V, Gould ES. Diffusion tensor imaging of peripheral nerves. *Skeletal Radiol* 2010; 39:1073–1079
39. Lehmann HC, Zhang J, Mori S, Sheikh KA. Diffusion tensor imaging to assess axonal regeneration in peripheral nerves. *Exp Neurol* 2010; 223: 238–244
40. Filler AG. Diagnosis and treatment of pudendal nerve entrapment syndrome subtypes: imaging, injections, and minimal access surgery. *Neurosurg Focus* 2009; 26:E9
41. Chappell KE, Robson MD, Stonebridge-Foster A, et al. Magic angle effects in MR neurography. *AJNR* 2004; 25:431–440
42. Grant GA, Britz GW, Goodkin R, Jarvik JG, Maravilla K, Kliot M. The utility of magnetic resonance imaging in evaluating peripheral nerve disorders. *Muscle Nerve* 2002; 25:314–331
43. Andreisek G, White LM, Kassner A, Tomlinson G, Sussman MS. Diffusion tensor imaging and fiber tractography of the median nerve at 1.5T: optimization of b value. *Skeletal Radiol* 2009; 38: 51–59
44. Ringleb SI, Bensamoun SF, Chen Q, Manduca A, An KN, Ehman RL. Applications of magnetic resonance elastography to healthy and pathologic skeletal muscle. *J Magn Reson Imaging* 2007; 25:301–309
45. Khalil C, Budzik JF, Kermarrec E, Balbi V, Le Thuc V, Cotten A. Tractography of peripheral nerves and skeletal muscles. *Eur J Radiol* 2010; 76:391–397
46. Yamashita T, Kwee TC, Takahara T. Whole-body magnetic resonance neurography. *N Engl J Med* 2009; 361:538–539
47. Wessig C, Bendszus M, Stoll G. In vivo visualization of focal demyelination in peripheral nerves by gadofluorine M-enhanced magnetic resonance imaging. *Exp Neurol* 2007; 204:14–19